

Role of chiral two-body currents in ${}^6\text{Li}$ magnetic properties in light of a new precision measurement with the relative self-absorption technique

U. Friman-Gayer,^{1,2,3,*} C. Romig,^{1,†} T. Hütter,¹ K. Albe,⁴ S. Bacca,^{5,6} T. Beck,¹ M. Berger,¹ J. Birkhan,¹ K. Hebeler,^{1,7} O. J. Hernandez,^{8,5} J. Isaak,¹ S. König,^{1,7,9} N. Pietralla,¹ P. C. Ries,¹ J. Rohrer,⁴ R. Roth,¹ D. Savran,¹⁰ M. Scheck,^{1,11,12} A. Schwenk,^{1,7,13} R. Seutin,^{13,1,7} and V. Werner¹

¹*Institut für Kernphysik, Technische Universität Darmstadt, 64289 Darmstadt, Germany*

²*Department of Physics and Astronomy, University of North Carolina at Chapel Hill, Chapel Hill, NC 27599, USA*

³*Triangle Universities Nuclear Laboratory, Duke University, Durham, NC 27708, USA*

⁴*Department of Materials Science, Technische Universität Darmstadt, 64287 Darmstadt, Germany*

⁵*Institut für Kernphysik and PRISMA Cluster of Excellence, Johannes Gutenberg-Universität Mainz, 55128 Mainz, Germany*

⁶*Helmholtz Institute Mainz, GSI Helmholtzzentrum für Schwerionenforschung GmbH, 64289 Darmstadt, Germany*

⁷*ExtreMe Matter Institute EMMI, GSI Helmholtzzentrum für Schwerionenforschung GmbH, 64289 Darmstadt, Germany*

⁸*Department of Physics and Astronomy, University of British Columbia, Vancouver BC, V6T 1Z4, Canada*

⁹*Department of Physics, North Carolina State University, Raleigh, NC 27695, USA*

¹⁰*GSI Helmholtzzentrum für Schwerionenforschung GmbH, 64289 Darmstadt, Germany*

¹¹*School of Engineering, University of the West of Scotland, Paisley, PA1 2BE, UK*

¹²*SUPA, Scottish Universities Physics Alliance, Glasgow, G12 8QQ, UK*

¹³*Max-Planck-Institut für Kernphysik, 69117 Heidelberg, Germany*

(Dated: January 8, 2021)

A direct measurement of the decay width of the excited 0_1^+ state of ${}^6\text{Li}$ using the relative self-absorption technique is reported. Our value of $\Gamma_{\gamma,0_1^+ \rightarrow 1_1^+} = 8.17(14)_{\text{stat.}}(11)_{\text{sys.}}$ eV provides sufficiently low experimental uncertainties to test modern theories of nuclear forces. The corresponding transition rate is compared to the results of *ab initio* calculations based on chiral effective field theory that take into account contributions to the magnetic dipole operator beyond leading order. This enables a precision test of the impact of two-body currents that enter at next-to-leading order.

Nuclear structure physics has entered an era of precision studies, both in experiment and theory. For light nuclei, *ab initio* theory based on interactions from chiral effective field theory [1] is reaching an accuracy at which corrections to electromagnetic (EM) operators which emerge naturally in the chiral expansion become relevant. A recent review [2] indicates that precision measurements of EM transition rates with uncertainties of a few percent or better are required to explore and validate the effects of these subleading corrections. For few-nucleon systems, direct measurements of strong transition rates with such precision are often challenging experimentally owing to the very short lifetimes involved.

The present study is focused on the nucleus ${}^6\text{Li}$ in its excited 0_1^+ state at $E_{0_1^+} = 3562.88(10)$ keV [3], which constitutes the lightest non-strange hadronic system [4] with a dominant internal EM decay branch to its 1_1^+ ground state. The potentially competing parity-forbidden decay via α emission has not been observed, and it is at least ten million times weaker than the γ decay [5]. Because of its occurrence as stable matter (compared to the lighter hypernuclei [6]) and the low nucleon number of ${}^6\text{Li}$, the decay of its 0_1^+ state is the EM transition of the simplest hadronic system which is simultaneously accessible by precision studies in theory and experiment. It is, therefore, ideally suited for testing our understanding of nuclear forces and EM currents in a many-nucleon system. Moreover, this is the EM-analog transition to the ${}^6\text{He}$ beta decay, whose rate was recently measured with

high precision [7], so that this $A = 6$ system in future offers a comprehensive test of electroweak interactions in light nuclei.

On the theory side, significant progress has been made in chiral effective field theory (χEFT) [1, 8], and in the *ab initio* solution of the quantum many-body problem for light nuclei [9, 10]. Recently, the focus has been on the consistent inclusion of electroweak transition operators [2], with a focus on the impact of two-body currents (2BC). For EM transitions in light nuclei, calculations with traditional 2BC and potentials were performed in Ref. [11], while calculations with 2BC from χEFT used in conjunction with wave functions derived from traditional potentials were performed in Ref. [12], reaching a precision at the few-percent level. In Ref. [13], this transition and the magnetic moment of the ground state of ${}^6\text{Li}$ were calculated with interactions from χEFT without 2BC. Similarly, these observables have been studied in Refs. [14–16]. In this work, we will present the first calculations obtained with 2BC and consistent interactions derived from χEFT . In the case of weak β decays, this has been shown to lead to a systematic improvement between experiment and theory [17].

From the experimental side, the determination of the isovector magnetic dipole transition strength $B(M1; 0_1^+, T=1 \rightarrow 1_1^+, T=0) \propto E_\gamma^{-3} \Gamma_{\gamma,0_1^+ \rightarrow 1_1^+}$ between the first excited 0_1^+ state of ${}^6\text{Li}$ with a total isospin quantum number of $T = 1$ and the $T = 0$ ground state, which is proportional to the product of the level width for γ

decay $\Gamma_{\gamma,0_1^+ \rightarrow 1_1^+}$ and a γ -ray energy (E_γ) dependent factor, has been the subject of considerable effort in the past. The extremely short half-life of the excited state of about 80 attoseconds (10^{-18} s) [3] makes a direct measurement of its decay rate impossible [18]. Panels (a)-(c) of Fig. 1 show the history of published values for this quantity as compiled in the Evaluated Nuclear Structure Data Files (ENSDF) [3]. They have been obtained using three different techniques, namely: nuclear resonance fluorescence relative to another transition (relative NRF) [19, 20], self absorption (SABs) [20–25], and inelastic electron scattering (e, e') [26–30]. In the ENSDF, a weighted average value of $B(M1)_{\text{ENSDF}} = 15.65(32) \mu_N^2$ {from $\Gamma_{\gamma,0_1^+ \rightarrow 1_1^+} = 8.19(17) \text{ eV}$ [3, 32]} is derived from a selection of three of the most recent publications in Ref. [33], meant to exclude earlier measurements with obvious systematic deviations (for comparison: a weighted average of all measurements yields a value of $B(M1) = 14.53_{-0.30}^{+0.20} \mu_N^2$). Regardless of the averaging procedure, the final result is strongly dominated by two (e, e') results of Eigenbrod [29] and, in particular, of Bergstrom *et al.* [30], which claim the highest precision. In such an (e, e') experiment, the $B(M1)$ value is obtained in a model-dependent way from the measured form factor $|F(q)|^2$, where q denotes the momentum transfer. Both works employed the plane-wave Born approximation to obtain the q -dependent $B(M1, q)$ from $|F(q)|^2$ [34], which is equal to the $B(M1)$ strength in the limit of the minimum necessary momentum transfer $q_0 = E_{0_1^+}/\hbar c \approx 0.018 \text{ fm}$, the so-called 'photon point'. Panel (d) of Fig. 1 shows $B(M1, q)$ values, obtained from the form factor of Bergstrom *et al.* [30], along with an uncertainty band from one possible extrapolation in our attempt to reproduce their results [31]. Similar to Refs. [29] and [30], the present extrapolations employed fits of low- q expansions of the model-independent energy dependence of the form factor with different cutoffs to varying subsets of the low- q data. In order to match the width of the uncertainty band to the datapoint of Bergstrom *et al.*, the selection of fits had to be limited to a reduced chi-square χ_ν^2 on the order of 0.1. It was found that the width of this band can easily be extended by increasing the cutoff or relaxing the restriction on χ_ν^2 . The obvious presence of systematic uncertainty in the literature data precludes a comparison to state-of-the-art theoretical results [2, 12] and calls for a precision measurement directly at the photon point to avoid the extrapolation uncertainty.

We have, therefore, performed an experiment to measure $\Gamma_{\gamma,0_1^+ \rightarrow 1_1^+}$ with the newly developed NRF-based relative SABs method [35, 36]. Compared to the traditional SABs technique [37] used in several previous experiments [20–25], it utilizes a normalization target (no) in combination with the scattering target of interest (sc) to sepa-

rate resonant and nonresonant processes¹:

$$R_{\text{exp}} = 1 - \left\langle \frac{N_{\text{no}}^{\text{nrf}}}{N_{\text{no}}^{\text{abs}}} \right\rangle \frac{N_{\text{sc}}^{\text{abs}}}{N_{\text{sc}}^{\text{nrf}}} = R \left(\Gamma_{\gamma,0_1^+ \rightarrow 1_1^+}, T_{\text{eff}} \right). \quad (1)$$

In Eq. (1), N_x^{nrf} denotes the number of observed NRF events from a γ -ray line from material x . The number of events is reduced to N_x^{abs} in a second measurement by the introduction of an absorber target, which consists of the same material as the scatterer of interest, into the incident continuous-energy photon beam. The reduction of the count rate of the NRF line of interest is due to nonresonant scattering as well as the SABs induced by the absorber. Both contributions can be separated in a model-independent way by using the reduction of the count rate in the NRF lines of the normalization target [factor $\langle N_{\text{no}}^{\text{nrf}}/N_{\text{no}}^{\text{abs}} \rangle$ in Eq. (1)], which is due to nonresonant effects, only. In the absence of other decay branches, R_{exp} is directly related to $\Gamma_{\gamma,0_1^+ \rightarrow 1_1^+}$ [37, 39] [see Eq. (1)], once the thermal motion of the nuclei of interest is taken into account. It can be treated in terms of an effective temperature T_{eff} [37, 39, 40] that includes corrections due to condensed-matter effects in the target material (see below).

The experiment was performed at the Darmstadt High-Intensity Photon Setup (DHIPS) [41], with continuous-energy photon beams generated by bremsstrahlung processes of a 7.1(2) MeV electron beam of the Superconducting Darmstadt Linear Accelerator (S-DALINAC) [42, 43] on a copper radiator. A scattering target composed of 5.033(5) g [particle areal density $d_{\text{sc,Li}} = 0.02773(6) \text{ b}^{-1}$, using a target diameter of 20.00(5) mm] of lithium carbonate (Li_2CO_3) enriched to 95.00(1) % in ^6Li , sandwiched between pure boron normalization targets of 2.118(5) g and 2.119(5) g with a 99.52(1) % ^{11}B enrichment, was measured for about 122 h. A second, 186 h, measurement was carried out with a 9.938(5) g [$d_{\text{abs,Li}} = 0.05469(10) \text{ b}^{-1}$] absorber of the same Li_2CO_3 material. Scattered γ rays from the target were detected by three high-purity germanium (HPGe) detectors at polar angles of 90° (twice) and 130° with respect to the beam axis. To avoid direct scattering of γ rays from the absorber target into the detectors, the target was mounted at the entrance of the 1 m-long collimation system of DHIPS, which acts as a passive shielding. The direct scattering into the detectors was found to be negligible by an additional 8 h measurement with the absorber target only. A potential systematic uncertainty due to small-angle scattering of bremsstrahlung γ rays inside the collimator, which would then induce excess NRF reactions in the scatterer, was found to be on the

¹ A detailed derivation of this equation can be found in the supplemental material [38]

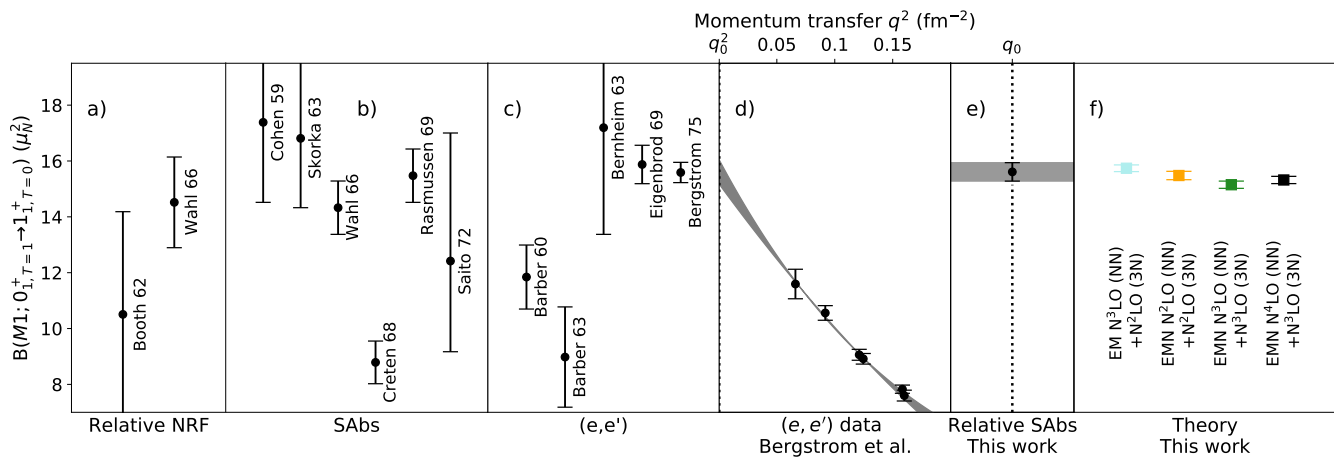


FIG. 1. (a-c): Previous measurements of the $B(M1; 1_1^+ \rightarrow 0_1^+)$ strength for ${}^6\text{Li}$ with the methods of relative NRF [19, 20] (a), SAbs [20–25] (b), and (e, e') [26–30] (c). For each experimental method, the data are sorted by the time of publication, with the most recent data point on the right. A label next to the data points indicates the year of publication and the last name of the first author. Low- q data of the most precise (e, e') result by Bergstrom et al. [30] and a possible quartic polynomial extrapolation (see also the supplemental material [31]) of $B(M1, q)$ to the photon point (q_0) are shown as an uncertainty band in (d). The present result, which can be interpreted as a measurement at q_0 , is given in panel (e). Panel (f) shows the result of four theoretical calculations from the present work (see also Fig. 3) with estimated uncertainties of the many-body method. They employed different Hamiltonians that are indicated by different colors and the labels below the data points and include the leading two-body currents.

order of 0.33% by GEANT4 [44–46] simulations (i.e., in the anticipated order of magnitude of the uncertainty of R) and taken into account by replacing $\langle N_{\text{no}}^{\text{nr}}/N_{\text{no}}^{\text{abs}} \rangle$ with $1.0033 \times \langle N_{\text{no}}^{\text{nr}}/N_{\text{no}}^{\text{abs}} \rangle$ in Eq. (1). Summed spectra of all three detectors from the measurements with and without absorber are provided in Fig. 2. Using the known inter-

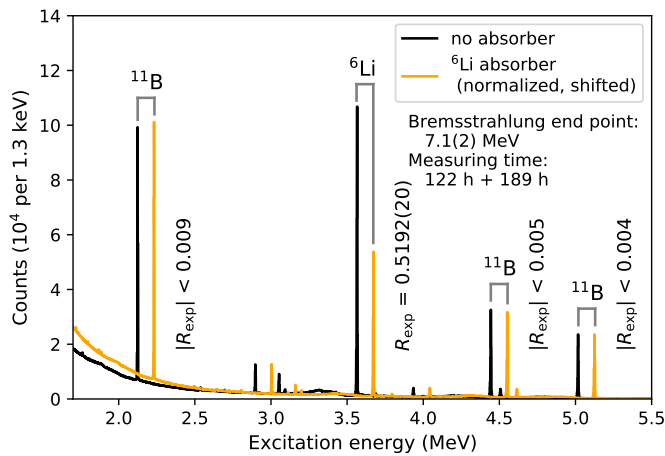


FIG. 2. Sum spectra of the three detectors from the measurement with (gold) and without (black) the ${}^6\text{Li}$ absorber. For better visibility, the spectrum with the absorber was shifted by 100 keV to higher energies. The observed NRF events of three transitions of ${}^{11}\text{B}$ were used to normalize the spectrum with the absorber, so that the difference in counts for the ${}^6\text{Li}$ transition is due to SAbs only. On the right-hand side of the transitions of interest, the (absolute) value of the SAbs (R_{exp}) is indicated, which is expected to be zero for ${}^{11}\text{B}$.

nal γ -ray transitions of ${}^{11}\text{B}$ at 2125, 4445, and 5020 keV [47], the measurement with the absorber was normalized to the one without it using the energy-dependent factor $N_{\text{no}}^{\text{nr}}/N_{\text{no}}^{\text{abs}}$ in Eq. (1). The normalization factor at the three discrete energies of the ${}^{11}\text{B}$ transitions were interpolated by a GEANT4 simulation of the γ -ray attenuation, which was in turn validated by an offline measurement with a radioactive ${}^{56}\text{Co}$ source. Including the counting statistics and the correction factor for small-angle scattering, and propagating uncertainties with a Monte-Carlo method [48], a value of $R_{\text{exp}} = 0.5192(20)$ with a relative uncertainty of 0.39% was obtained.

Li_2CO_3 was chosen as the target material to reduce systematic uncertainties because pure lithium, used in all previous experiments [19–30], is highly hygroscopic, which may lead to systematic errors in the determination of the target thickness. The T_{eff} value for Li_2CO_3 [see Eq. (1)] was determined from state-of-the-art atomic theory. First, the phonon density of states (phDOS) of Li_2CO_3 was obtained from density functional theory (DFT) [49, 50]. Computations of this observable are typically in excellent agreement with experimental data [51, 52]. The DFT calculations employed the GPAW [53, 54] code in a plane-wave basis. For the exchange-correlation (xc) potential, the local-density (LDA) [55] and the generalized-gradient approximation (GGA) [56] were tried, which typically slightly under- (LDA) and overestimate (GGA) the crystal binding. Both xc potentials reproduced the experimental lattice constants a, b, c , and γ of Li_2CO_3 [57] with deviations at the 0.1% level; this can be viewed as a

benchmark test. From the phDOS, a value of $T_{\text{eff}} = 411(11)\text{K}$ was obtained by the procedure described in Ref. [40], which represents the average value and spread of the LDA and GGA solutions. Using all the aforementioned input [58], our experimental value for the γ -decay width is $\Gamma_{\gamma,0^+ \rightarrow 1^+} = 8.17_{-0.13}^{+0.14}$ (stat.) $_{-0.11}^{+0.10}$ (syst.) eV, which corresponds to a strength $B(M1;0^+ \rightarrow 1^+) = 15.61_{-0.25}^{+0.27}$ (stat.) $_{-0.21}^{+0.19}$ (syst.) μ_N^2 . The 68.3% coverage interval (CI) is divided into statistical (stat) and systematic (syst) parts, where the latter account for uncertainties in the target dimensions as well as in atomic and condensed-matter contributions².

For the *ab initio* calculations, the importance-truncated no-core shell model (IT-NCSM) [59, 60] was employed as a state-of-the-art many-body method. Within the IT-NCSM, two-nucleon (NN) and three-nucleon (3N) interactions derived within χ EFT were used. Four different Hamiltonians (I-IV) were considered, including (I) the Entem-Machleidt (EM) NN interaction at N³LO [61], complemented with a local 3N interaction (cutoff $\Lambda = 500$ MeV, $c_D = 0.8$) at N²LO, which is fitted to reproduce the binding energy as well as the β -decay half-life of ³H [62, 63]. Furthermore, Hamiltonians (II-IV) use the NN interactions by Entem, Machleidt and Nosyk (EMN) at N²LO, N³LO and N⁴LO with $\Lambda = 500$ MeV [8], complemented with consistent nonlocal 3N interactions up to N²LO, N³LO and N³LO, respectively. The NN interactions were only fitted to NN scattering data and the deuteron binding energy, while the 3N interactions were fitted to reproduce the triton binding energy and to optimize the ground-state energy and radius of ⁴He, which led to the values $c_D = -1$, $c_D = 2$ and $c_D = 3$, for the cases II, III and IV, respectively. The similarity renormalization group (SRG) was employed at the NN and 3N level with a flow parameter of $\alpha = 0.08$ fm⁴ [64, 65].

Using an SRG-transformed Hamiltonian requires a consistent SRG transformation of the $M1$ operator. In previous studies [13–16], this consistent treatment was neglected, here SRG corrections of the $M1$ operator were included at the two-body level. In addition to the SRG correction, the NLO 2BC contributions to the $M1$ operator were included as well. At NLO, these are commonly expressed as a sum of two contributions, the *intrinsic* term and the *Sachs* term [66]:

$$\mu_{[12]}^{\text{NLO}}(\mathbf{R}, \mathbf{k}) = \mu_{[12]}^{\text{intrinsic}}(\mathbf{k}) + \mu_{[12]}^{\text{Sachs}}(\mathbf{R}, \mathbf{k}) \quad (2)$$

² Since both contributions are uncorrelated and the CIs are almost symmetric, a symmetrized and quadratically summed uncertainty of $15.61(33)\mu_N^2$ is used in all figures.

TABLE I. Results of the theoretical calculations for $B(M1;0^+_{1,T=1} \rightarrow 1^+_{1,T=0})$ and $\mu(1^+_{1,T=0})$ of ⁶Li. These employed four different Hamiltonians (I-IV), which are introduced in the text. The calculations are sorted by the type of $M1$ operator, with the same abbreviations as in Fig. 3. For comparison, the results of QMC calculations in Refs. [11, 12] are shown in the second part of the Table. The 'standard nuclear physics approach' (SNPA) for the operator in Ref. [11] was complemented by a χ EFT approach in Ref. [12], while in both cases phenomenological potentials were used. 'LO' refers to one-body currents and 'Total' to the inclusion of two-body currents.

	I	II	III	IV
	LO			
μ (μ_N)	0.8399(22)	0.8374(24)	0.8344(21)	0.8388(18)
$B(M1)$ (μ_N^2)	15.02(10)	14.92(13)	14.68(10)	14.81(10)
	LO SRG ev.			
μ (μ_N)	0.8221(28)	0.8195(29)	0.8188(26)	0.8236(23)
$B(M1)$ (μ_N^2)	14.44(8)	14.36(11)	14.13(8)	14.32(8)
	NLO SRG ev.			
μ (μ_N)	0.8240(34)	0.8216(34)	0.8217(32)	0.8261(28)
$B(M1)$ (μ_N^2)	15.74(12)	15.48(15)	15.15(13)	15.32(13)
	[11]		[12]	
	QMC LO			
	SNPA		χ EFT	
μ (μ_N)	0.810(1)		0.817(1)	
$B(M1)$ (μ_N^2)	12.84(11)		–	
	QMC Total			
μ (μ_N)	0.800(1)		0.807(1)	
$B(M1)$ (μ_N^2)	15.00(11)		–	

with

$$\mu_{[12]}^{\text{intrinsic}}(\mathbf{k}) = -\frac{i}{2}\nabla_{\mathbf{q}} \times \mathbf{J}(\mathbf{q}, \mathbf{k})|_{\mathbf{q}=0}$$

$$\mu_{[12]}^{\text{Sachs}}(\mathbf{R}, \mathbf{k}) = -\frac{i}{2}e(\boldsymbol{\tau}_1 \times \boldsymbol{\tau}_2)_z \mathbf{R} \times \nabla_{\mathbf{k}}v(\mathbf{k}).$$

Here, $\boldsymbol{\tau}_i$ are the Pauli matrices, \mathbf{q} the momentum transfer of the photon, $v(\mathbf{k})$ the one-pion exchange potential in momentum representation, and \mathbf{R} the center of mass coordinate of the two nucleons. The Sachs term only depends on the potential between the two nucleons, whereas the translationally-invariant intrinsic term is given by the spatial part of the two-body current \mathbf{J} . For each interaction, an IT-NCSM calculation was carried out with N_{max} from 2 to 12 with harmonic-oscillator frequencies $\hbar\Omega = 16, 20, 24$ MeV. For the resulting value of the magnetic moment and the transition strength, the central value for the highest N_{max} was used as the nominal result, and the neighboring results as an estimate for the many-body uncertainties. The results of the calculations are listed in Tab. I and displayed in Fig. 3 [see also panels (e) and (f) of Fig. 1], where they are compared to the new experimental constraint of the present work and the magnetic moment $\mu(1^+_{1,T=0}) = 0.82205667(26)\mu_N$ [3] of the ground state of ⁶Li.

Remarkably, the results of the most complete calculations, including contributions from the 2BC to the $M1$

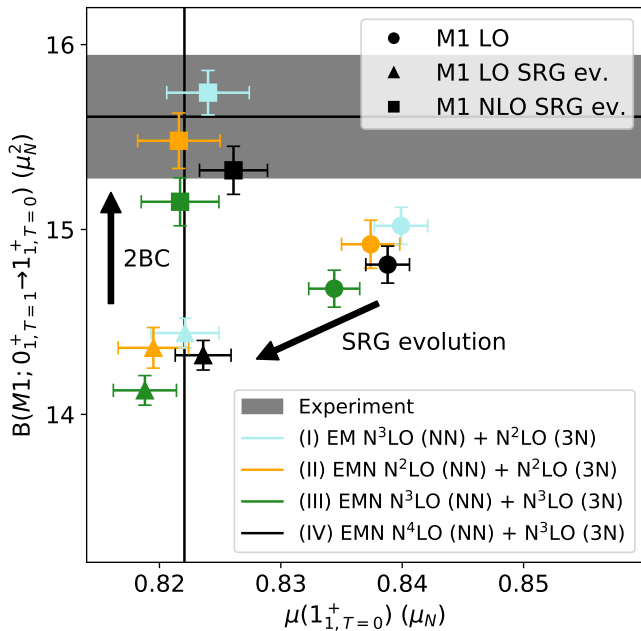


FIG. 3. Results for $B(M1; 0_{1,T=1}^+ \rightarrow 1_{1,T=0}^+)$ and $\mu(1_{1,T=0}^+)$ from theoretical calculations based on Hamiltonians I-IV (see also Tab. I). As shown in the upper legend, circular markers indicate calculations with the unevolved leading-order (LO) one-body transition operator, triangular markers indicate calculations with the consistently SRG-transformed operator (LO SRG ev.), and quadratic markers indicate the calculations with a consistently SRG-transformed operator including contributions from next-to-leading order 2BC (NLO SRG ev.). The labeled arrows illustrate the impact of the two aforementioned improvements. Figure 1 shows only the results with the most complete transition operator in the same color code. The experimental 68% CI for $B(M1)$ (present work) is indicated by a shaded area, and the most probable values of $B(M1)$ and μ [3] by a solid line (the CI of μ is not visible at this scale).

operator, exhibit an excellent agreement with the new experimental constraints of the present work. This indicates the importance of 2BC for a correct description of the ${}^6\text{Li}$ nucleus. The residual differences between experiment and theory are probably related to missing higher-order contributions to the $M1$ operator. The increase of the $B(M1)$ strength is also found in quantum Monte Carlo (QMC) calculations when 2BC are included [11, 12] (see also Tab. I).

In contrast to the data points that presently dominate the world average, this measurement was performed directly at the photon point and with controlled systematic uncertainties. In total, a relative uncertainty of 2% with balanced contributions by statistics and systematics was achieved. This translates into an uncertainty of about 2 attoseconds for the half-life of the 0_1^+ state of ${}^6\text{Li}$. In addition, χEFT nuclear structure calculations were performed which take into account 2BC at NLO, combined

with chiral interactions at various orders, for the first time. Excellent agreement between experiment and theory was found at a new level of precision in both areas.

ACKNOWLEDGMENTS

We thank the crew of the S-DALINAC for providing excellent conditions for experimentation. This work was supported by the Deutsche Forschungsgemeinschaft (DFG) under grants No. SFB 634 (Project ID 5485852), SFB 1044 (204404729), SFB 1245 (279384907), and the Cluster of Excellence PRISMA⁺ (39083149), by the Bundesministerium für Bildung und Forschung under grant No. 05P18PKEN9, and by the State of Hesse within the LOEWE research project 'Nuclear Photonics'. Numerical calculations have been performed on the LICHTENBERG cluster at the computing center of the TU Darmstadt. This material is based upon work supported by the U.S. Department of Energy, Office of Science, Office of Nuclear Physics, under the FRIB Theory Alliance award DE-SC0013617. MB, PCR, TB, and UFG acknowledge support by the Helmholtz Graduate School for Hadron and Ion Research of the Helmholtz Association. RS acknowledges support by the International Max Planck Research School for Precision Tests of Fundamental Symmetries.

* ufrimangayer@ikp.tu-darmstadt.de

† Present address: Projektträger DESY, Deutsches Elektronen-Synchrotron, 22607 Hamburg, Germany

- [1] E. Epelbaum, H. W. Hammer, and U.-G. Meißner, Modern theory of nuclear forces, *Rev. Mod. Phys.* **81**, 1773 (2009).
- [2] S. Bacca and S. Pastore, Electromagnetic reactions on light nuclei, *J. Phys. G* **41**, 123002 (2014).
- [3] D. R. Tilley, C. M. Cheves, J. L. Godwin, G. M. Hale, H. M. Hofmann, J. H. Kelley, C. G. Sheu, and H. R. Weller, Energy levels of light nuclei $A=5, 6, 7$, *Nucl. Phys. A* **708**, 3 (2002).
- [4] P. A. Zyla, R. M. Barnett, J. Beringer, O. Dahl, D. A. Dwyer, D. E. Groom, C. J. Lin, K. S. Lugovsky, E. Pianori, D. J. Robinson, *et al.* (Particle Data Group), Review of Particle Physics, *Prog. Theor. Exp. Phys.* **083C01**, 1 (2020).
- [5] R. G. H. Robertson, P. Dyer, R. C. Melin, T. J. Bowles, A. B. McDonald, G. C. Ball, W. G. Davies, and E. D. Earle, Upper limit on the isovector parity-violating decay width of the 0^+ $T = 1$ state of ${}^6\text{Li}$, *Phys. Rev. C* **29**, 755 (1984).
- [6] O. Hashimoto and H. Tamura, Spectroscopy of Δ hypernuclei, *Prog. Part. Nucl. Phys.* **57**, 564 (2006).
- [7] A. Knecht, R. Hong, D. W. Zumwalt, B. G. Delbridge, A. García, P. Müller, H. E. Swanson, I. S. Towner, S. Utsumo, W. Williams, and C. Wrede, Precision measurement of the ${}^6\text{He}$ half-life and the weak axial current in nuclei, *Phys. Rev. Lett.* **108**, 122502 (2012).

- [8] D. R. Entem, R. Machleidt, and Y. Nosyk, High-quality two-nucleon potentials up to fifth order of the chiral expansion, *Phys. Rev. C* **96**, 024004 (2017).
- [9] B. R. Barrett, P. Navrátil, and J. P. Vary, Ab initio no core shell model, *Prog. Part. Nucl. Phys.* **69**, 131 (2013).
- [10] J. Carlson, S. Gandolfi, F. Pederiva, S. C. Pieper, R. Schiavilla, K. E. Schmidt, and R. B. Wiringa, Quantum Monte Carlo methods for nuclear physics, *Rev. Mod. Phys.* **87**, 1067 (2015).
- [11] L. E. Marcucci, M. Pervin, S. C. Pieper, R. Schiavilla, and R. B. Wiringa, Quantum Monte Carlo calculations of magnetic moments and $M1$ transitions in $A \leq 7$ nuclei including meson-exchange currents, *Phys. Rev. C* **78**, 065501 (2008).
- [12] S. Pastore, S. C. Pieper, R. Schiavilla, and R. B. Wiringa, Quantum Monte Carlo calculations of electromagnetic moments and transitions in $A \leq 9$ nuclei with meson-exchange currents derived from chiral effective field theory, *Phys. Rev. C* **87**, 035503 (2013).
- [13] A. Calci and R. Roth, Sensitivities and correlations of nuclear structure observables emerging from chiral interactions, *Phys. Rev. C* **94**, 014322 (2016).
- [14] N. M. Parzuchowski, S. R. Stroberg, P. Navrátil, H. Hergert, and S. K. Bogner, Ab initio electromagnetic observables with the in-medium similarity renormalization group, *Phys. Rev. C* **96**, 034324 (2017).
- [15] I. J. Shin, Y. Kim, P. Maris, J. P. Vary, P. Forssén, J. Rotureau, and N. Michel, Ab initio no-core solutions for ${}^6\text{Li}$, *J. Phys. G* **44**, 075103 (2017).
- [16] S. Binder, A. Calci, E. Epelbaum, R. J. Furnstahl, J. Golak, K. Hebeler, T. Hüther, H. Kamada, H. Krebs, P. Maris, U.-G. Meißner, A. Nogga, R. Roth, R. Skibiński, K. Topolnicki, J. P. Vary, K. Vobig, and H. Witała (LENPIC Collaboration), Few-nucleon and many-nucleon systems with semilocal coordinate-space regularized chiral nucleon-nucleon forces, *Phys. Rev. C* **98**, 014002 (2018).
- [17] P. Gysbers, G. Hagen, J. D. Holt, G. R. Jansen, T. D. Morris, P. Navrátil, T. Papenbrock, S. Quaglioni, A. Schwenk, S. R. Stroberg, and K. A. Wendt, Discrepancy between experimental and theoretical β -decay rates resolved from first principles, *Nature Phys.* **15**, 428 (2019).
- [18] P. J. Nolan and J. F. Sharpey-Schafer, The measurement of the lifetimes of excited nuclear states, *Rep. Prog. Phys.* **42**, 1 (1979).
- [19] E. Booth and K. A. Wright, Nuclear resonance scattering of Bremsstrahlung, *Nucl. Phys.* **35**, 472 (1962).
- [20] S. J. Skorka, J. Hertel, and T. W. Retz-Schmidt, Compilation of electromagnetic transition rates in light nuclei ($A \leq 40$), *Nucl. Data Sheets A* **2**, 347 (1966); H. Wahl *et al.* (1966), (unpublished).
- [21] L. Cohen and R. A. Tobin, Lifetime of the 3.56-MeV state of Li^6 , *Nucl. Phys.* **14**, 243 (1959).
- [22] S. J. Skorka and R. Hübner and T. W. Retz-Schmidt and H. Wahl, Width of the 3.56 MeV ($T = 1$) level in Li^6 , *Nuclear Physics* **47**, 417 (1963).
- [23] W. L. Creten, R. J. Jacobs, and H. M. Ferdinande, Widths of low-lying levels of ${}^6\text{Li}$, *Nuclear Physics A* **120**, 126 (1968).
- [24] V. K. Rasmussen and C. P. Swann, Gamma-Ray Widths in C^{13} , Li^6 , and P^{31} , *Phys. Rev.* **183**, 918 (1969).
- [25] T. Saito, Resonance Scattering of Bremsstrahlung by ${}^6\text{Li}$, ${}^{11}\text{B}$ and ${}^{27}\text{Al}$, *J. Phys. Soc. Jpn.* **35**, 1 (1973).
- [26] W. C. Barber, F. Berthold, G. Fricke, and F. E. Gudden, Nuclear Excitation by Scattering of 40-Mev Electrons, *Phys. Rev.* **120**, 2081 (1960).
- [27] W. C. Barber, J. Goldemberg, G. A. Peterson, and Y. Torizuka, Study of nuclear magnetic transitions by inelastic electron scattering, *Nucl. Phys.* **41**, 461 (1963).
- [28] M. Bernheim and G. Bishop, Excitation of levels in $\text{Li}6$ by inelastic electron scattering, *Phys. Lett.* **5**, 270 (1963).
- [29] F. Eigenbrod, Untersuchung der vier ersten angeregten Zustände des ${}^6\text{Li}$ -Kernes durch Elektronenstreuung, *Z. Phys.* **228**, 337 (1969).
- [30] J. Bergstrom, I. Auer, and R. Hicks, Electroexcitation of the 0^+ (3.562 MeV) level of ${}^6\text{Li}$ and its application to the reaction ${}^6\text{Li}(\gamma, \pi^+){}^6\text{He}$, *Nucl. Phys. A* **251**, 401 (1975).
- [31] (), see Supplemental Material at [URL will be inserted by publisher] for an attempt of the authors of the present article to reconstruct the analysis of the electron scattering data of Ref. [30].
- [32] F. Ajzenberg-Selove, Energy levels of light nuclei $A = 5-10$, *Nucl. Phys. A* **490**, 1 (1988).
- [33] F. Ajzenberg-Selove, Energy levels of light nuclei $A = 5-10$, *Nucl. Phys. A* **320**, 1 (1979).
- [34] H. Theissen, Spectroscopy of light nuclei by low energy (< 70 MeV) inelastic electron scattering, in *Springer Tr. Mod. Phys.*, Vol. 65 (Springer Berlin Heidelberg, 1972) pp. 1–57.
- [35] C. Romig, D. Savran, J. Beller, J. Birkhan, A. Endres, M. Fritzsche, J. Glorius, J. Isaak, N. Pietralla, M. Scheck, L. Schnorrenberger, K. Sonnabend, and M. Zweidinger, Direct determination of ground-state transition widths of low-lying dipole states in ${}^{140}\text{Ce}$ with the self-absorption technique, *Phys. Lett. B* **744**, 369 (2015).
- [36] C. Romig, *Investigation of Nuclear Structure with Relative Self-Absorption Measurements*, Ph.D. thesis, Technische Universität Darmstadt, Darmstadt (2015).
- [37] F. R. Metzger, Resonance Fluorescence in Nuclei, *Prog. Nucl. Phys.* **7**, 53 (1959).
- [38] (), see Supplemental Material at [URL will be inserted by publisher] for more details on the relative self absorption.
- [39] N. Pietralla, I. Bauske, O. Beck, P. von Brentano, W. Geiger, R.-D. Herzberg, U. Kneissl, J. Margraf, H. Maser, H. H. Pitz, *et al.*, Absolute level widths in ${}^{27}\text{Al}$ below 4 MeV, *Phys. Rev. C* **51**, 1021 (1995).
- [40] W. E. Lamb, Capture of neutrons by atoms in a crystal, *Phys. Rev.* **55**, 190 (1939).
- [41] K. Sonnabend, D. Savran, J. Beller, M. A. Büssing, A. Constantinescu, M. Elvers, J. Endres, M. Fritzsche, J. Glorius, J. Hasper, J. Isaak, B. Löher, S. Müller, N. Pietralla, C. Romig, A. Sauerwein, L. Schnorrenberger, C. Wälzlein, A. Zilges, and M. Zweidinger, The Darmstadt High-Intensity Photon Setup (DHIPS) at the S-DALINAC, *Nucl. Instrum. Meth. A* **640**, 6 (2011).
- [42] A. Richter, Operational Experience at the S-DALINAC, in *Proc. EPAC'96* (1996).
- [43] N. Pietralla, The Institute of Nuclear Physics at the TU Darmstadt, *Nucl. Phys. News* **28**, 4 (2018).
- [44] S. Agostinelli, J. Allison, K. Amako, J. Apostolakis, H. Araujo, P. Arce, M. Asai, D. Axen, S. Banerjee, G. Barrand, *et al.*, Geant4-a simulation toolkit, *Nucl. Instrum. Meth. A* **506**, 250 (2003).
- [45] J. Allison, K. Amako, J. Apostolakis, H. Araujo, P. A. Dubois, M. Asai, G. Barrand, R. Capra, S. Chauvie, R. Chytráček, *et al.*, Geant4 developments and applications, *IEEE T. Nucl. Sci.* **53**, 270 (2006).

- [46] J. Allison, K. Amako, J. Apostolakis, P. Arce, M. Asai, T. Aso, E. Bagli, A. Bagulya, S. Banerjee, G. Barrand, *et al.*, Recent developments in Geant4, Nucl. Instrum. Meth. A **835**, 186 (2016).
- [47] J. H. Kelley, E. Kwan, J. E. Purcell, C. G. Sheu, and H. R. Weller, Energy levels of light nuclei $A=11$, Nucl. Phys. A **880**, 88 (2012).
- [48] Joint Committee for Guides in Metrology, *Evaluation of measurement data - Guide to the expression of uncertainty in measurement* (JCGM100, 2008).
- [49] P. Hohenberg and W. Kohn, Inhomogeneous Electron Gas, Phys. Rev. **136**, B864 (1964).
- [50] W. Kohn and L. J. Sham, Self-Consistent Equations Including Exchange and Correlation Effects, Phys. Rev. **140**, A1133 (1965).
- [51] X. Gonze and C. Lee, Dynamical matrices, born effective charges, dielectric permittivity tensors, and interatomic force constants from density-functional perturbation theory, Phys. Rev. B **55**, 10355 (1997).
- [52] S. Baroni, S. de Gironcoli, A. Dal Corso, and P. Giannozzi, Phonons and related crystal properties from density-functional perturbation theory, Rev. Mod. Phys. **73**, 515 (2001).
- [53] J. J. Mortensen, L. B. Hansen, and K. W. Jacobsen, Real-space grid implementation of the projector augmented wave method, Phys. Rev. B **71**, 035109 (2005).
- [54] J. Enkovaara, C. Rostgaard, J. J. Mortensen, J. Chen, M. Dułak, L. Ferrighi, J. Gavnholt, C. Glinsvad, V. Haikola, H. A. Hansen, *et al.*, Electronic structure calculations with GPAW: a real-space implementation of the projector augmented-wave method, J. Phys.-Condens. Mat. **22**, 253202 (2010).
- [55] J. P. Perdew and Y. Wang, Accurate and simple analytic representation of the electron-gas correlation energy, Phys. Rev. B **45**, 13244 (1992).
- [56] J. P. Perdew, K. Burke, and M. Ernzerhof, Generalized gradient approximation made simple, Phys. Rev. Lett. **77**, 3865 (1996).
- [57] H. Effenberger and J. Zemann, Verfeinerung der Kristallstruktur des Lithiumkarbonates, Li_2CO_3 , Z. Kristallogr. **150**, 133 (1979).
- [58] (), see Supplemental Material at [URL will be inserted by publisher] for a detailed account of the experimental uncertainty.
- [59] R. Roth, Importance truncation for large-scale configuration interaction approaches, Phys. Rev. C **79**, 064324 (2009).
- [60] R. Roth and P. Navrátil, Ab initio study of ^{40}Ca with an importance-truncated no-core shell model, Phys. Rev. Lett. **99**, 092501 (2007).
- [61] D. R. Entem and R. Machleidt, Accurate charge-dependent nucleon-nucleon potential at fourth order of chiral perturbation theory, Phys. Rev. C **68**, 041001(R) (2003).
- [62] D. Gazit, S. Quaglioni, and P. Navrátil, Three-Nucleon Low-Energy Constants from the Consistency of Interactions and Currents in Chiral Effective Field Theory, Phys. Rev. Lett. **103**, 102502 (2009).
- [63] D. Gazit, S. Quaglioni, and P. Navrátil, Erratum: Three-Nucleon Low-Energy Constants from the Consistency of Interactions and Currents in Chiral Effective Field Theory [Phys. Rev. Lett. 103, 102502 (2009)], Phys. Rev. Lett. **122**, 029901(E) (2019).
- [64] R. Roth, J. Langhammer, A. Calci, S. Binder, and P. Navrátil, Similarity-transformed chiral $nn + 3n$ interactions for the ab initio description of ^{12}C and ^{16}O , Phys. Rev. Lett. **107**, 072501 (2011).
- [65] R. Roth, A. Calci, J. Langhammer, and S. Binder, Evolved chiral $nn + 3n$ hamiltonians for ab initio nuclear structure calculations, Phys. Rev. C **90**, 024325 (2014).
- [66] S. Pastore, L. Girlanda, R. Schiavilla, M. Viviani, and R. B. Wiringa, Electromagnetic currents and magnetic moments in chiral effective field theory (χEFT), Phys. Rev. C **80**, 034004 (2009).